Chapter 18

Fiber Lasers in Material Processing

Catherine Wandera

Additional information is available at the end of the chapter

http://dx.doi.org/10.5772/62014

Abstract

The economic aspects of laser usage in manufacturing that form important criteria in the choice of a suitable laser system for thick-section metal cutting include: high processing speeds, high processing depths, high cut edge quality, and high wall-pug efficiency of the laser system. Consequently, the performance of the high brightness ytterbium fiber laser system in thick-section metal cutting is evaluated based on the maximum achievable cutting speeds, maximum cutting depths possible, and cut edge quality attainable. The maximum processing speeds, maximum processing depths, and resulting cut edge quality are governed by a number of parameters related to the laser system, workpiece specification, and the cutting process. The effects of the processing parameters in the cutting of thick-section stainless steel and mild steel and medium-section aluminium have been reported; optimization of the processing parameters for enhancement of the cut edge quality has been discussed.

Keywords: Ytterbium Fiber Laser, Thick-section Metal, Cutting

1. Introduction

1.1. The high-power fiber laser

The development in the output power of solid-state fiber laser source has resulted in the increasing interest in the use of the high brightness fiber laser in macro laser material processing applications, especially cutting and welding of metal [1]. The essence of the design of the high-power fiber laser (a solid-state laser) is the improved cooling of the laser-active medium which enables attainment of higher output power with high beam quality. Among the rare earth ions used in fiber lasers, ytterbium is highly absorbing of pump radiation and is preferred as doping material for the high-power fiber laser operating at 1,060–1,080 nm spectral range and delivering kilowatt output power suitable for material processing [2].

1.2. The structure of the ytterbium fiber laser

The structure of the high-power ytterbium fiber laser includes a double-clad glass fiber having a core region in which the laser-active ytterbium ions are deposited. The core region of highest refractive index is surrounded by two cladding regions of progressively decreasing refractive index which serve to confine the pump light within the core region. The ytterbium ion-doped core region is surrounded by an inner cladding of lower refractive index than the core and the inner cladding is in turn surrounded by an outer cladding of still lower refractive index forming a step index fiber (see Figure 1a). The pump light from high-power laser diode arrays is guided into the inner cladding (referred to as pump cladding), and this pump light is confined in the inner cladding by the lower refractive index outer cladding (see Figure 1b). The confinement of pump light rays within the fiber core region – subject to some losses through absorption or scattering – maintains the pump light intensity propagating in the fiber over a fiber length of several meters. Subsequently, the pump light propagating in the fiber is absorbed by the laser-active ytterbium ions in the core region of the fiber, resulting in the lasing action of the ytterbium ions. The stimulated emission resulting from the lasing action is guided inside the core region building up to high intensities before it finally emerges as a high-power laser beam at near-infrared spectral range of 1,060–1,080nm [3, 4, 5]. The small core diameter of single-mode fibers (3–10 μm) ensures that the power density of the output beam is very high. The use of cladding-pumping in the high-power ytterbium fiber laser limits the thermal issues (i.e., the variation of the refractive index with temperature) that affect the stability of high-power Nd: YAG lasers [6]. The temperature in the fiber core is determined primarily by heat transport through the outer surface of the fiber [7]; the geometry of the fiber laser exposes a large surface area per unit volume, which aids the cooling of fiber lasers [8]. Therefore, the improved cooling mechanism in the ytterbium fiber laser has enabled the solid-state laser to achieve near diffraction limited beam quality at high output power [3].

1.3. Fiber laser features beneficial to materials processing

The high brightness ytterbium fiber laser operating at 1,060–1,080 nm spectral range has a unique combination of high-power output, high beam quality, and near-infrared wavelength, and these characteristics offer increased performance flexibility in materials processing applications. Consequently, the solid-state ytterbium fiber laser has introduced solid-state laser sources to the material processing applications – such as thick-section metal cutting and welding – that had previously been considered impractical for the traditional solid-state Nd: YAG laser due to its limited beam quality at high output power [3, 4, 9, 10, 11, 12].

1.3.1. Output power

The availability of high-power diode lasers as pumping sources for fiber lasers and improvements in fiber laser design have enabled power scaling of ytterbium (Yb^{3+})-doped fiber lasers to output powers beyond 1 kW in *cw* operation with near diffraction-limited beam quality [8, 13]. Additionally, laser beam combination techniques are also used for power scaling of the ytterbium fiber laser by bundling multiple single-mode fiber laser elements to provide up to

http://dx.doi.org/10.5772/62014

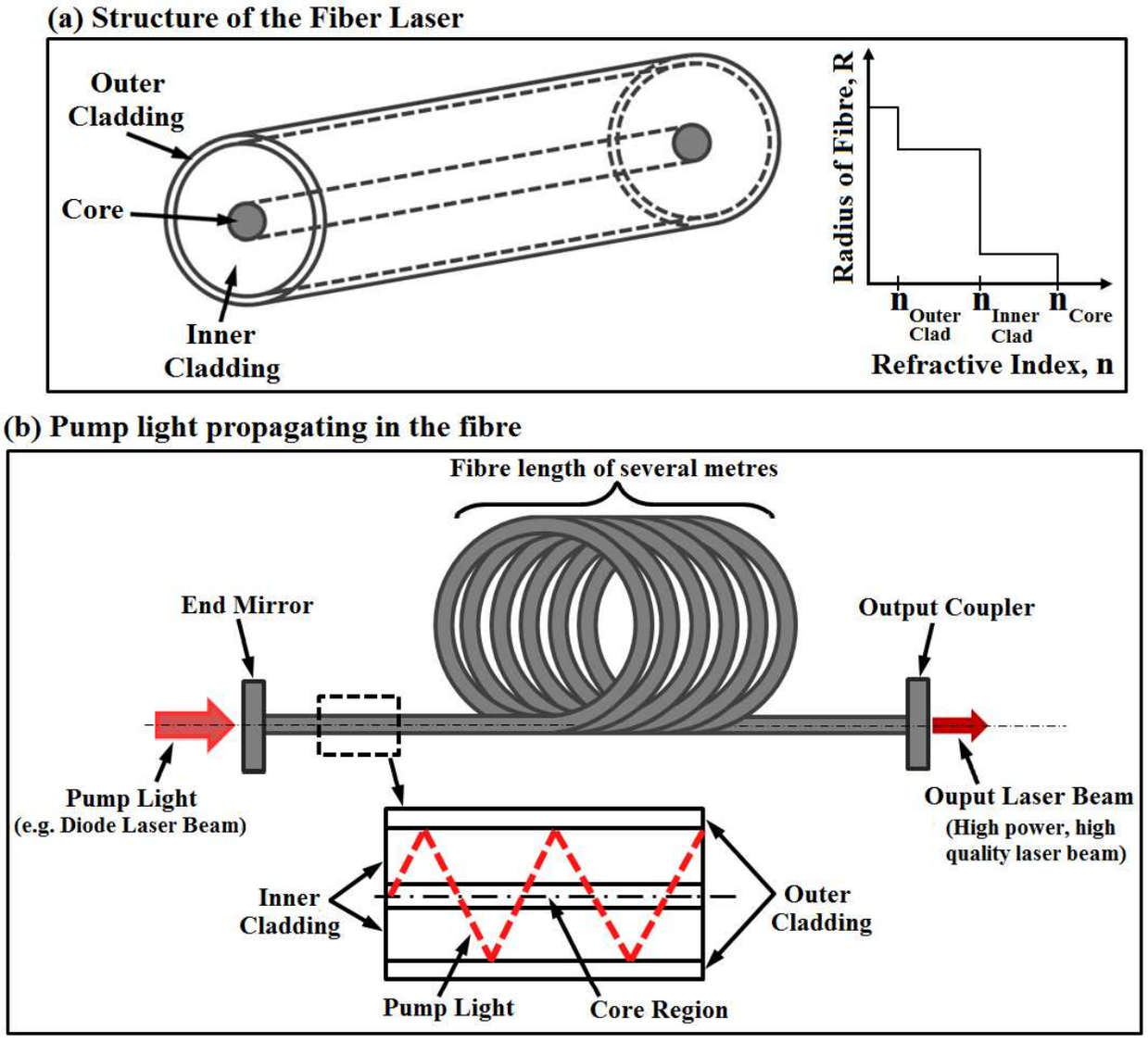

Figure 1. A schematic illustration of the double-clad fiber

10 kW multi-mode power output. Consequently, ytterbium fiber lasers delivering over 10 kilowatt power output are now available for materials processing applications [14].

1.3.2. Laser beam quality and focusing

The performance of the high-power ytterbium fiber laser in materials processing applications is enhanced by its high beam quality at high output power, which results in high brightness. The quality of a laser beam is characterized by the beam parameter product (BPP), which is the standard measure of beam quality that incorporates the wavelength effects. The beam parameter product (BPP) – defined by the relationship in Equation (1) – is an important parameter for the comparison of the beam quality of laser beams of different wavelengths from different laser sources. In the relation given in Equation (1), λ is the wavelength of the laser beam and M^2 is the beam quality factor (i.e., times diffraction limit factor) which tells how

much larger the BPP of the laser beam under consideration is compared to the lowest value of λ / π for the basic Gaussian TEM_{00} mode (diffraction limit) [3, 15].

$$BPP = \frac{\lambda}{\pi} \cdot M^2 \tag{1}$$

Focusability of the laser beam is an important requirement for its utilization in cutting and welding applications. The laser beam quality is the critical parameter that influences the focusability of the laser beam; Equation (2) gives the relationship between the BPP of the laser beam and the minimum focused spot size, d_f for focusing optics of focal length, f, and a raw beam diameter on the focusing optics, D. [3, 15]. Near diffraction limited beam quality (i.e., high beam quality denoted by low BPP) is essential for focusing of the laser beam to a small focal spot size to give very high power intensity necessary for processing of thick-section metals at the required high processing speed. The high power intensity enables melting of the workpiece at the laser-material interaction zone at a high processing speed [16].

$$d_f = \frac{4f}{D} \cdot BPP \tag{2}$$

The depth of focus – i.e., the effective distance over which the minimum focused beam diameter is maintained – is the distance over which the power intensity is maximum and satisfactory cutting can be achieved. A longer depth of focus is essential for good cut edge quality like in thick-section metal cutting. For a given laser beam quality, Equation (3) gives the relationship between the focal length of the focusing optics, f, and the depth of focus, d_Z, which shows that use of a longer focal length focusing optics increases the depth of focus [3]. However, the minimum focused spot size is also directly proportional to the focal length (see Equation (2)) such that use of longer focal length optics for focusing of the laser beam results in a larger focused spot size with reduced power intensity. Therefore, the low BPP of the high brightness fiber laser beam allows the use of long focal length focusing optics for achievement of a long depth of focus and long working distance without much compromise on the minimum focused spot size.

$$d_Z = 4\left(\frac{f}{D}\right)^2 \times BPP \tag{3}$$

where: d_Z is the depth of focus, f is the focal length of the focusing optics, D is the raw beam diameter on the focusing optics, and BPP is the beam parameter product of the incident laser beam.

1.3.3. Wavelength

Absorption of the laser beam by metals increases for wavelengths toward the visible and ultraviolet regions and decreases towards the longer infrared wavelengths. The near infrared

wavelength of the high brightness ytterbium fiber laser offers a higher absorptivity by metals than the CO_2 laser. The more energetic photons of the shorter wavelength radiation of the ytterbium fiber laser can be absorbed by a greater number of electrons in the metal structure such that the reflectivity of the metal surface falls and absorptivity is greatly increased [15]. Additionally, the fiber laser wavelength offers lower sensitivity to laser-induced plasmas during materials processing when compared to the CO_2 laser. The inverse bremsstrahlung absorption by the plasma produced during laser welding is lower with the 1.06 μm wavelength radiation of the solid-state Nd: YAG laser than with the 10.6 μm radiation of the CO_2 laser [15]. Furthermore, fiber laser beam wavelength offers more flexible beam handling through use of narrow optical fibers.

2. Absorption of the laser beam by metals

The focused high-intensity laser beam radiation that is incident on the surface of a metal workpiece is partly absorbed and partly reflected by the metal surface. In a laser cutting or welding process, a sufficient amount of the focused laser beam incident on a metal workpiece must be absorbed by the workpiece so as to cause melting of the material in the laser beam–material interaction zone at the desired processing speed.

2.1. Mechanisms of laser beam absorption

Laser cutting and welding of metals require absorption of high power intensities to enhance cutting and welding at high processing speeds. The two absorption mechanisms that prevail during cutting and welding of metal include *Fresnel absorption* and *plasma absorption* (inverse bremsstrahlung effect); these laser beam absorption mechanisms are explained in the following sections.

2.1.1. Fresnel absorption mechanism

The direct absorption of the beam by the workpiece takes place through the Fresnel absorption mechanism (i.e., absorption during reflection from the surface). Fresnel absorption occurs during direct interaction of the beam and the material in which the photons of the incident laser beam radiation are absorbed by the free electrons in the metal structure. The absorbed energy sets the electrons in forced vibration motion which can be detected as heat. Absorption increases with increase in temperature of the material due to an increase in the phonon population causing more phonon–electron energy exchanges and more tendencies for the electrons to interact with the material structure with the resultant fall in reflectivity [15].

2.1.2. Plasma absorption mechanism

Plasma absorption mechanism (i.e., inverse bremsstrahlung effect) occurs when there is presence of laser-induced plasma during the process. Plasma absorption occurs through absorption of the laser beam by the free electrons in the plasma (i.e., hot metal vapor) leading

to plasma re-radiation [15]. The two methods of welding of metal using a laser beam include: *conduction limited welding* and *keyhole welding*. Conduction limited welding occurs when the power density is not sufficient to cause evaporation of part of the melt at the given welding speed. Keyhole welding occurs when the energy is sufficient to cause boiling and evaporation of part of the melt creating a hole (referred to as keyhole) in the melt pool and plasma (metal vapor) [17, 18]; the keyhole is stabilized by the pressure from the vapor generated. The plasma in the keyhole consists of both vapor from the evaporated melt of the metal being welded and the shroud gas sucked into the hot vapor due to the pulsation of the keyhole. The absorption of the laser beam within the keyhole is through both Fresnel absorption (i.e., absorption directly by the material) and plasma absorption (i.e., inverse bremsstrahlung effect) by the free electrons in the metallic plasma. Consequently, the presence of plasma interferes with the laser beam delivery to the interaction zone by blocking the beam through beam-scattering effects caused by changes in refractive index and particles caught up in the plasma [15].

2.2. Laser beam absorption during metal cutting

The melt film in the cutting front is generated by the melting action of the absorbed laser beam power and the oxidation reaction power (in the case of oxygen or compressed air assist gas). Initiation of laser cutting of metals by piercing of the workpiece with a focused incident laser beam to generate a melt surface throughout the workpiece thickness is affected by metal surface reflectivity. The surface reflectivity limits the amount of laser energy coupled to the workpiece; therefore, metals with high surface reflectivity – e.g., aluminum – require higher power intensity for cut initiation. After the initiation of cutting, the cutting process progresses by the laser beam absorption on the steeply sloped cut front by the two absorption mechanisms, namely Fresnel absorption and plasma absorption and re-radiation (15). However, the plasma buildup is not very significant in cutting due to the assist gas which blows it away; therefore, plasma absorption mechanism is very limited in laser cutting. With absorption of sufficient laser energy, the thermal vibrations in the metal become so intense that the molecular bonding is stretched and is no longer capable of exhibiting mechanical strength, resulting in melting of the metal at the interaction zone. Olsen [19, 20], in his description of the mechanisms of the cutting front formation, identified the *melt surface*, *melt film*, and *melt front* as the three zones that comprise the cutting front. After cut initiation, the laser cutting process proceeds through absorption of the incident laser beam at the melt surface; the absorbed laser beam is transmitted to the melt front through the melt film. There is a minimum melt film thickness necessary for transmission of the absorbed energy from the melt surface to the melt front. The melt surface propagates through the material with a velocity that depends on the energy input, thermal properties of the workpiece material, and the molten material removal mechanisms. The melt front velocity increases with increasing laser power intensity which enhances the penetration speed [21]. Multiple reflections of the incident laser beam inside thick-section cut kerfs result in increased absorption of the beam inside the cut kerf; consequently, the maximum temperature in the cutting front occurs below the material surface. Multiple reflections of the laser beam inside the cut kerf increase with increasing workpiece thickness and cutting speed because the multiple reflections are a function of the cutting depth and cutting front inclination [22].

http://dx.doi.org/10.5772/62014

3. Laser cutting of thick-section metals

Laser cutting of metals requires very high power intensities (intensities of the magnitude 10^{10} W/m^2) to melt the metallic material to the required penetration depth at a high cutting speed. Therefore, the material's surface reflectivity, thermal conductivity, and workpiece thickness are the material parameters that critically affect the efficiency of the laser cutting process. The speed of penetration of a metal workpiece during laser cutting depends on the absorbed incident laser power intensity. Therefore, the ease with which a metallic material can be cut depends on the absorptivity of the material to the incident laser beam, and the melting temperature of the material or oxide formed when a reactive assist gas is used [15].

3.1. Applicable laser cutting methods

Laser fusion cutting using an inert gas or an active gas is commonly used in thick-section metal cutting. Due to the high power requirement for vaporization cutting, this cutting method is not applicable to thick-section metal cutting. Figure 2 schematically illustrates the cut kerf generated and the volume of material removed during laser fusion cutting of thick-section metal. The cut kerf is the opening that is created during through-thickness penetration of a workpiece; therefore, the cut kerf width, w, shown in Figure 2 is the separation distance between the two cut surfaces of the cut kerf which represents the amount of material removed during the laser cutting process.The laser power absorbed at the cutting front is utilized in melting the kerf volume at the rate of cutting and part of the absorbed laser power is lost from the cutting zone through heat conduction to the substrate metal. The maximum cutting speed that can be applied on a given metal thickness is influenced by the laser power intensity that is available for melting of the kerf volume at the applied cutting speed. Consequently, penetration of a metal workpiece of a given thickness may not be achievable at cutting speeds beyond the maximum cutting speed for the applied laser power intensity.

3.1.1. Laser fusion cutting using an inert assist gas jet

The principle role of the inert assist gas jet – e.g., nitrogen – during laser cutting of a metal workpiece is to eject the molten metal to create the cut kerf. Metallic materials like stainless steel and aluminium are often laser cut using an inert assist gas jet (usually nitrogen) to give clean unoxidized cut edges which do not require any cleaning operation after cutting. The inert gas-assisted laser fusion cutting process utilizes a focused high-intensity laser beam to melt the kerf volume and a coincident high-pressure inert gas jet to blow out the molten metal to form a cut kerf. In this cutting process, the melt temperature is not raised to boiling point; and the melt removal process is solely dependent on the drag force supplied by the high pressure assist gas jet. During inert gas-assisted laser fusion cutting of metal, the absorbed laser power is the only incoming power contribution to the cutting zone. The absorbed laser power is utilized in both melting the workpiece material equivalent to the kerf volume and accounting for the inevitable power losses from the cutting zone. Therefore, in a pure laser fusion cutting process – typical for thick-section metal cutting – where the kerf volume is melted but

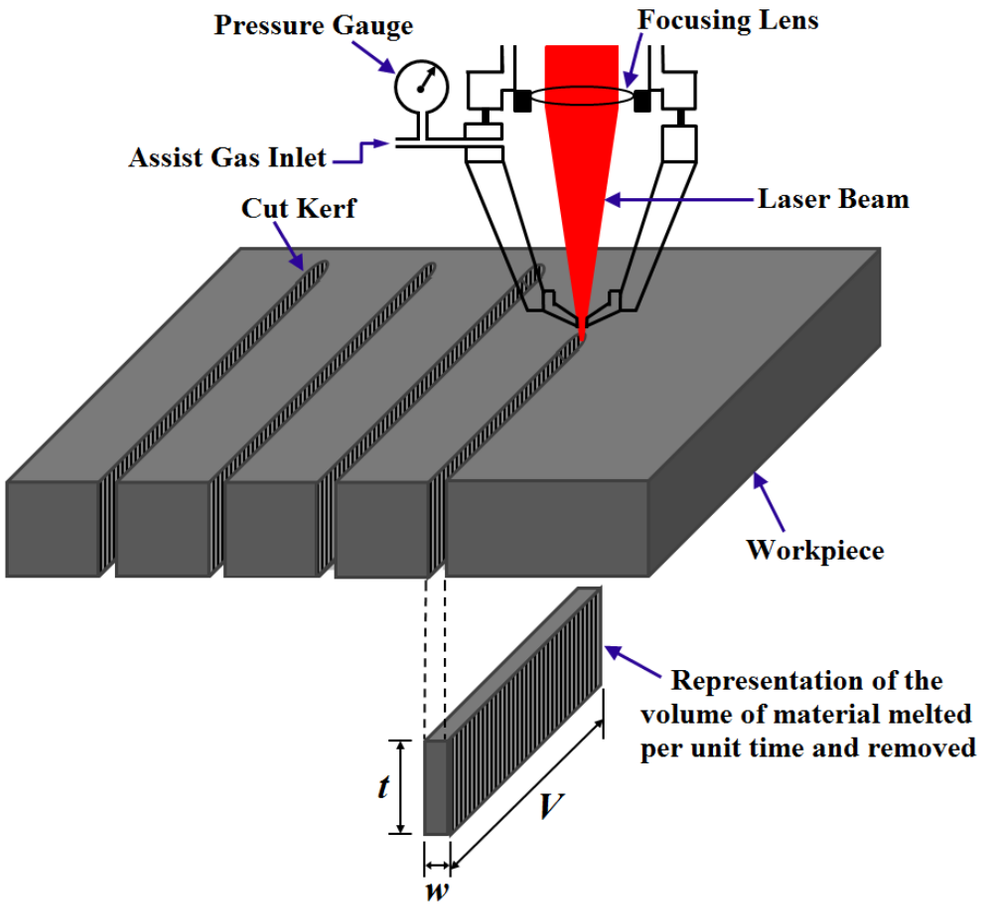

Figure 2. Cut kerf generated and the volume of material removed

negligibly vaporized and the conduction power losses from the cutting zone are significant, the power balance at the cutting front is given in Equation 4 [15].

$$A P_L = P_{Melt} + P_{Loss} \tag{4}$$

where A is the absorptivity of the workpiece to the incident laser radiation, P_L is the incident laser power, P_{Melt} is the power utilized in melting the kerf volume, and P_{Loss} is the inevitable power loss from cutting zone.

In examining the power requirement during laser cutting of a metal workpiece using inert and oxidizing assist gas jets, Wandera et al. [23] developed a theoretical model to estimate the power requirement for melting the kerf volume and the inevitable conduction power losses. Schulz et al. [24] developed an analytical approximation of the heat conduction losses during laser cutting of metals and provided an expression that can be used to estimate the temperature change in the substrate metal during laser cutting; the temperature change in the substrate metal is inversely proportional to the Peclet number which is directly proportional to the cutting speed.

http://dx.doi.org/10.5772/62014

3.1.2. Reactive fusion cutting

Reactive fusion cutting utilizes an active assist gas jet (usually oxygen or compressed air) that is capable of reacting exothermically with the molten metal and the reaction generates an additional heat source to the cutting process [15, 25]. The two major roles of an active assist gas jet (oxygen or compressed air) during laser cutting of a metal are to influence the energy balance at the cutting zone through the exothermic oxidation reaction and also eject the oxidized molten metal. The exothermic oxidation reaction contributes up to 40% of the energy used in the laser cutting of mild steel and stainless steel using oxygen assist gas jet [15].

During reactive fusion cutting, the incident laser beam melts the workpiece and also ignites and carries on the exothermic reaction between the molten metal and the active gas jet. Therefore, the active assist gas jet passing through the cut kerf plays two important roles which include exerting the necessary drag force to blow the molten material out the cut kerf and providing additional heat to the cutting process. Consequently, for the same incident laser power, cutting speeds of the reactive fusion cutting using an active (oxygen or compressed air) assist gas are usually higher compared to the inert gas-assisted cutting process. The incoming power contributions to the cutting zone during active gas-assisted laser cutting of metal include the absorbed laser power and the power from the exothermic oxidation reaction. In reactive fusion cutting of thick-section metal, the proportion of the kerf volume that is vaporized is considered to be negligible due to the high conduction losses which scale up with increase in workpiece thickness. The conduction heat transfer from the cutting front through the kerf walls to the substrate metal is the significant means of power loss from the laser–material interaction zone (i.e., cutting zone).

Iron-oxide (FeO) generated in oxygen-assisted laser cutting of mild steel does not boil, but would dissociate when heated to high temperatures; the iron-oxide dissociation process which consumes much energy could lead to a collapse of the cutting process [26]. Therefore, it is sufficient to assume that molten metal oxide is removed through the bottom of the cut kerf without vaporization. The oxidation of the metal melt during laser cutting is sustained in as much as the reactants - i.e., O_2 and molten metal – are available in the laser material interaction zone. Therefore, the power contribution to the cutting process by the oxidation reaction (i.e., reaction power) is estimated from either the oxygen flow into the interaction zone or the molten iron flow into the interaction zone [27]. The extent of the exothermic reaction in the cutting front is limited by the flow rate of the rarer type of reactant (either oxygen or iron). Only a small proportion of the oxygen jet is consumed in the oxidation reaction as part of the oxygen jet is utilized as drag to accelerate the melt out of the cut kerf while part of it is lost across the top workpiece surface or down the kerf; consequently, only about 50% of the molten iron reacts with the oxygen in the cut kerf. The cutting speeds in reactive fusion cutting are much higher than in fusion cutting with an inert assist gas because of the additional heat added by the exothermic reaction. Due to the high productivity of the reactive fusion cutting, this method is often used in industry for cutting of mild steel (i.e., low alloy steel). The presence of the oxide layer on the cut edge is the downside of this process as the oxide layer on the cut edge influences the final quality of the part; this oxide layer may require to be removed in a cleaning operation prior to further processing of the part in welding and painting operations.

3.2. Absorptivity (coupling coefficient) and melting efficiency

Absorptivity, A (also known as absorption coefficient), of the metal surface to the laser radiation is defined as the ratio of the laser power absorbed at the surface to the incident laser power. Absorptivity depends on the wavelength of laser radiation, plane of polarization of the light beam, angle of incidence, material type, and temperature and state of the material (solid, liquid, or gas). For an opaque material such as a metal, the absorptivity is given as $A=1-R$, where R is the reflectivity of the workpiece surface. Absorptivity of the light beam by the metal workpiece generally increases with increase in the temperature of the metallic material. When the angle of incidence is zero (i.e., vertical incidence), the parallel polarized laser beam (R_P) and the perpendicularly polarized laser beam (R_s) are absorbed equally. However, the absorption coefficient of the parallel polarized light (R_P) increases with increase in angle of incidence and is highest at the Brewster angle while the absorption coefficient of the perpendicularly polarized light (R_s) decreases with increase in angle of incidence [25, 27, 28].

The absorptivity (coupling coefficient), A, of the workpiece to the incident laser beam can be estimated by considering that the absorbed laser power is utilized to account for both the melting of the kerf volume and the inevitable conduction power losses. For a pure fusion cutting process utilizing only the incident laser power as the incoming power source, the absorptivity (coupling coefficient) of the workpiece to the incident laser radiation can be estimated using Equation 6.

$$A = \frac{Absorbed\ \ Laser\ Power\left(AP_L\right)}{Incident\ \ Laser\ Power\left(P_L\right)} = \frac{\left(P_m + P_{Losss}\right)}{P_L} \tag{5}$$

$$A = \frac{\left[\rho w t V\left(C_P \Delta T + L_m\right)\right] + \left[2\left(\rho C_P \Delta T_{Loss} V L t\right)\right]}{P_L} \tag{6}$$

where A is the absorptivity of the workpiece to the incident laser radiation; P_L is the incident laser power, (W); P_m is the laser power for melting the kerf volume, (W); P_{Loss} is the inevitable power loss from cutting zone (W); w is the kerf width, (m); t is the workpiece thickness, (m); V is the cutting speed, (m/s); ρ is the metal workpiece density, (kg/m^3); C_P is the specific heat capacity of the material, (J/kg/K); ΔT is the temperature rise to cause melting of kerf volume, (K) ; L_m is the latent heat of melting of the material (J/kg); ΔT_{Loss} is the temperature change in the substrate metal (K).

3.3. Melt removal during laser cutting

In laser cutting of metal, the cut kerf is created by continuously shearing and acceleration of the molten metal out of the cutting front by action of the drag force of the high pressure assist gas jet acting coaxially with the laser beam. The efficiency of melt removal from the cut kerf

http://dx.doi.org/10.5772/62014

during laser cutting of a metal workpiece plays a very important role on the cutting performance and the resulting cut edge quality. A minimum melt film thickness should be maintained at the cutting front to enhance efficient energy coupling to the unmelted metal in the line of traverse of the laser beam for continued cutting. Molten metals that have high surface tension and high viscosity are more difficult to remove from the cutting front and have a high tendency to attach on the underside of the cut as dross. Thus, the quality of the cut depends on the quantity of the melt which builds up in the cut kerf and causes dross on the cut surface.

3.3.1. Melt flow velocity and melt film thickness

The molten metal ejection is mainly driven by the shear force at the assist gas–melt interface and the pressure gradient created in the cut kerf. With the coaxial arrangement of the assist gas nozzle with the incident laser beam, the entire melt surface in the cut kerf is in contact with the assist gas jet. The cut kerf width is usually a fraction of a millimeter and the molten metal has a high viscosity such that the melt flow can be assumed to cover the entire cut kerf. Consequently, the expression for the melt flow can be analyzed by applying the principles of conservation of mass and momentum to the boundary layer flow of the melt film.

Wandera and Kujanpää [29] modeled the maximum melt flow velocity, U, at the gas–melt interface and the melt film thickness, t_{melt} under high pressure inert assist gas processing conditions as presented in Equations 7 and 8, respectively. The characteristic gas velocity, U_g, inside the cut kerf is estimated using the Bernoulli equation as presented in Equation 9. During laser fusion cutting using an inert assist gas jet, the molten metal has a high viscosity such that high assist gas pressure is required to facilitate high melt flow velocity, ensuring a minimal melt film thickness and achievement of high cut edge quality.

$$U = \left(\frac{1}{\eta + \mu}\right)\left(\frac{\rho_g U_g^{\,2}}{16t}\right)w^2 \tag{7}$$

$$t_{melt} = \frac{24\,V\,d^2\left(\eta + \mu\right)}{\rho_g U_g^{\,2} w^2} \tag{8}$$

$$P = \frac{\rho_g U_g^{\,2}}{2} \tag{9}$$

where U is the maximum melt flow velocity; η is the gas viscosity; μ is the melt kinematic viscosity ; ρ_g is the gas density; U_g is the characteristic gas velocity inside the cut kerf; t is the workpiece thickness ; w is the kerf width; t_{melt} is the melt film thickness; V is the cutting speed; d is the workpiece thickness; P is assist gas pressure.

The variation of melt flow velocity and melt film thickness along the cut depth is shown in Figure 3. There is retardation of the melt as the melt flow progresses down the cut kerf,

resulting in the melt buildup at the lower section of the cut kerf and subsequently dross attachment on the lower cut edge. The melt flow velocity increases with increase in assist gas pressure and increase in the cut kerf width, resulting in a reduction in the melt film thickness.

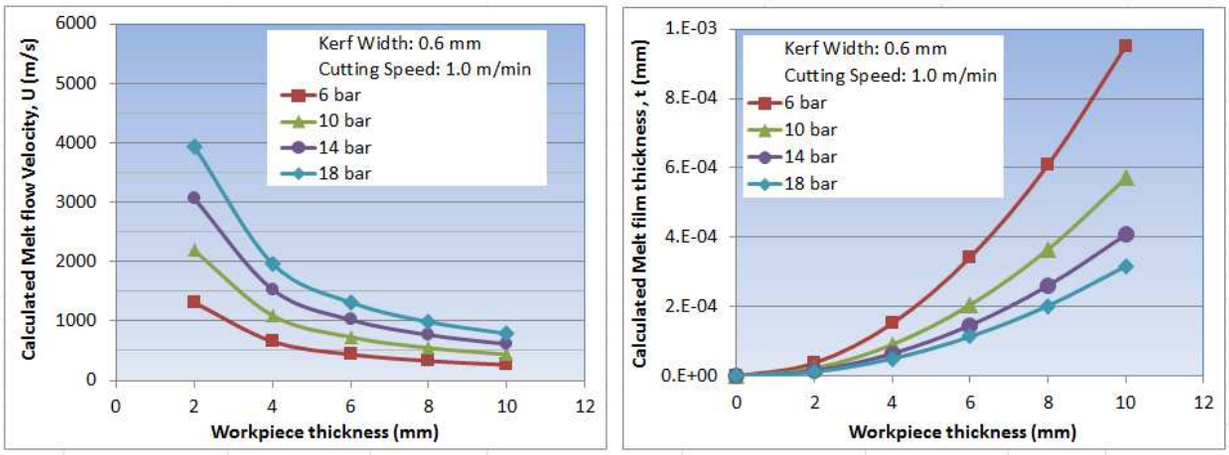

Figure 3. Variation of melt flow velocity and melt film thickness with cut depth for different assist gas pressure.

3.3.2. Separation and transition of melt flow

The retardation of the viscous melt streamlines during laser cutting of a thick-section metal using an inert assist gas jet can result in flow separation as the melt layer thickens rapidly in order to satisfy continuity within the boundary layer. The point along the cut edge where the flow separation occurs is referred to as the boundary layer separation point (BLS), which is shown in Figure 4. Downstream from the boundary layer separation point, there is a back-flow of the melt adjacent to the kerf wall and the boundary layer flow transitions from a laminar flow into a turbulent flow in which the melt particles move in random paths. The transition to turbulent boundary layer flow can also be caused by the disturbances in the laser cutting process – e.g., fluctuations in processing parameters – which may become amplified until turbulence is developed [30].

4. Performance of fiber lasers in metal cutting

The evaluation of the performance of the high brightness ytterbium fiber laser system in thick-section metal cutting is based on the maximum achievable cutting speeds, maximum cutting depths possible, and cut edge quality attainable. The maximum processing speeds, maximum processing depths, and resulting cut edge quality are governed by a number of parameters related to the laser system, workpiece specification, and the cutting process [15]. For cutting of a specific metal of a given thickness, the cutting process parameters can be altered by the operator so as to optimize the cutting process and obtain high cut quality at an optimal cutting speed for high productivity.

http://dx.doi.org/10.5772/62014

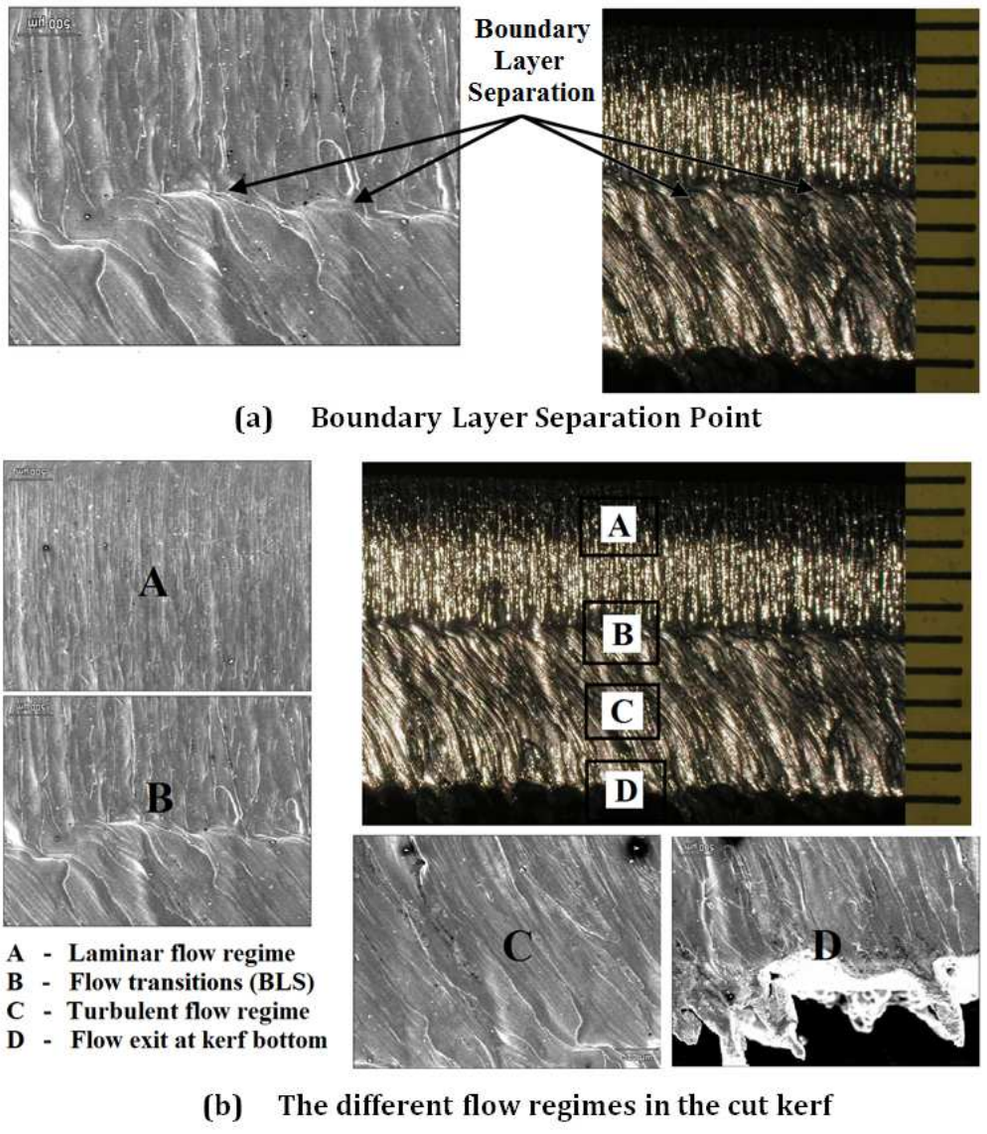

Figure 4. SEM image of the boundary layer separation on a 10-mm stainless steel cut edge

4.1. Maximum achievable cutting speed

The maximum achievable cutting speed for a given laser power level is the maximum cutting speed at which the cut edges are separated. Wandera et al. [23, 31] tested the maximum cutting speeds with the corresponding required laser power levels for the cutting of 10-mm stainless steel, 15-mm mild steel, and 4-mm aluminium using the fiber laser as presented in Figure 5. Using 5 kW fiber laser power, stainless steel of 10-mm thickness can be cut at a maximum cutting speed of 1.5 m/min with nitrogen assist gas jet and mild steel of 15-mm thickness can be cut at a cutting speed of 1.8 m/min with oxygen assist gas jet. Aluminium of 4-mm workpiece thickness can be cut at 10.2 m/min using 5 kW fiber laser power and nitrogen assist gas jet. A comparison of the fiber laser and CO_2 laser cutting speeds in cutting of 15-mm mild steel and 10-mm stainless steel showed that the fiber laser cutting speeds were over 1.3 times higher than the CO_2 laser cutting speeds for the same power level (see Figure 6). And in the cutting

of 6–10-mm stainless steel, Sparkes et al. [32] reported an increase in fiber laser cutting speeds of up to 1.5 times higher than the CO_2 laser cutting speeds. Wandera et al. [33] also investigated the cutting of 1–6-mm stainless steel using a fiber laser of beam quality 2.5mm.mrad and reported more than double increase in cutting speeds in 1–4-mm workpiece thickness compared to the CO_2 laser cutting speeds. The cutting speed difference between the fiber laser and the CO_2 laser reduces with increase in metal workpiece thickness to the thick-section domain. The increased cutting speeds for fiber laser is an indication of a higher absorption of the fiber laser beam by the metal workpiece compared to the absorption of the CO_2 laser beam. The melting efficiency of a given laser increases with increase in the absorptivity since a larger proportion of the incident laser radiation is absorbed by the material and utilized in melting of the kerf volume during cutting. Due to the reduction in the proportion of the absorbed laser beam that is lost through conduction to the substrate metal with higher cutting speeds, the potential increase in cutting speed when using the high-power ytterbium fiber laser increases the melting efficiency because the conduction energy losses from the cutting front decrease with increase in cutting speed.

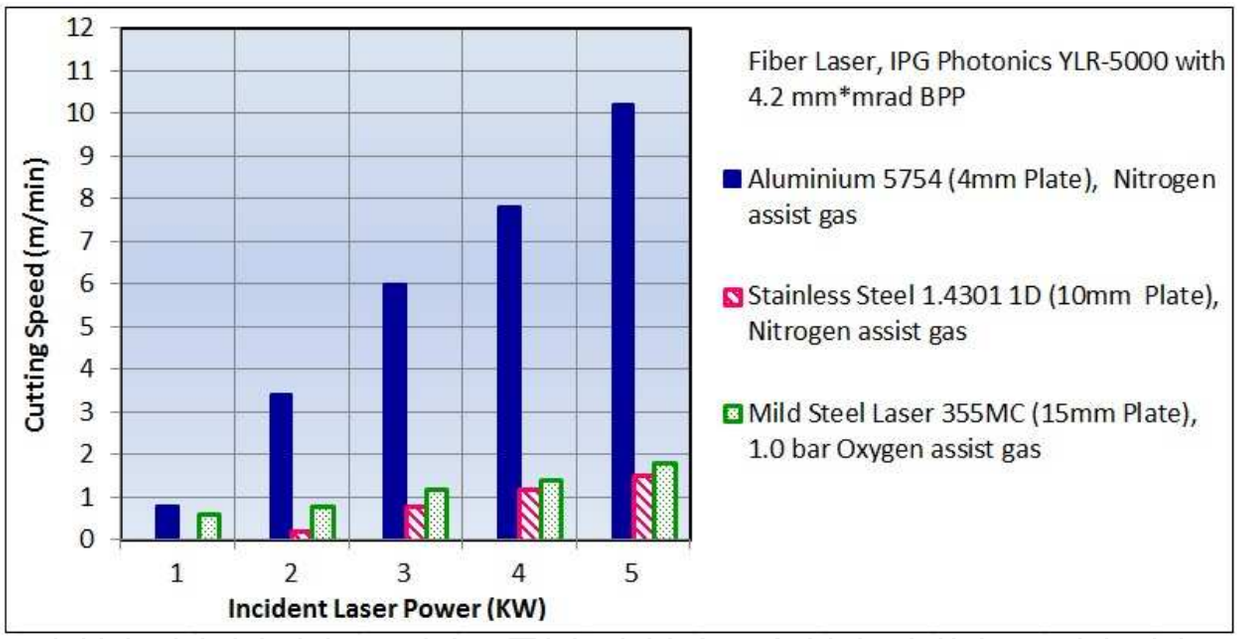

Figure 5. Maximum achievable cutting speeds using the ytterbium fiber laser

4.2. Cut quality characterization

According to the ISO standard for classification of thermal cuts (SFS-EN ISO 9013:2002) [34], the cut edge characteristics that are used to classify thermal cuts include: surface roughness and perpendicularity (squareness) deviation. Dross adherence and presence of the boundary layer separation on the laser cut edges which affect the surface roughness characteristic of a laser cut edge are critical quality aspects that need to be considered in thick-section metal laser cutting.

http://dx.doi.org/10.5772/62014

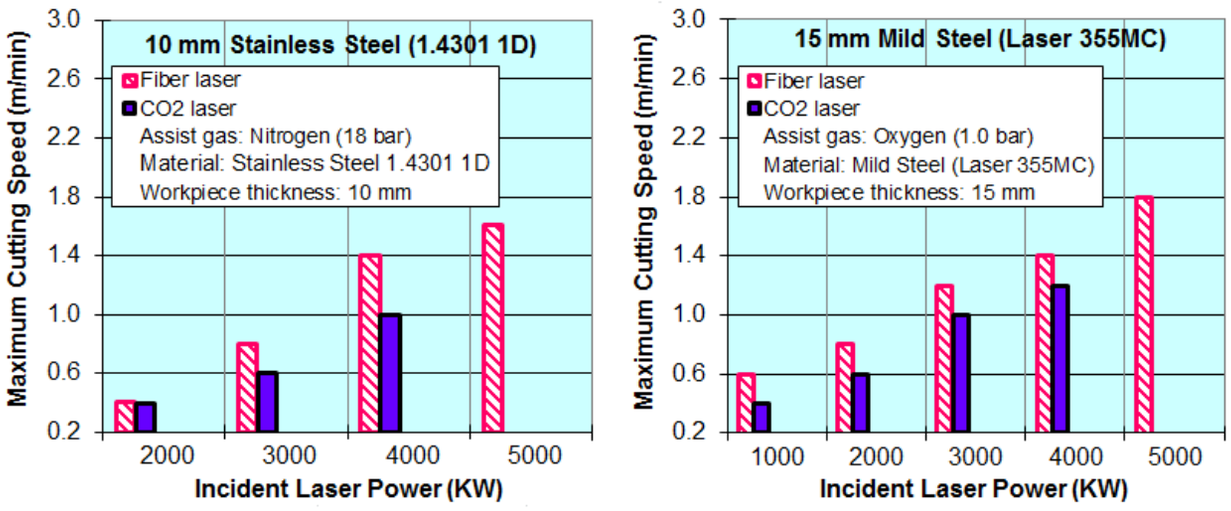

Figure 6. Maximum cutting speeds for cutting 10-mm stainless steel and 15-mm mild steel

4.2.1. Boundary layer separation and dross adherence

The presence of the boundary layer separation and dross adherence on the laser cut edge are characteristics of poor cut edge quality. The tendency of boundary layer separation and dross adherence on cut edges during thick-section metal cutting using an inert assist gas is influenced by the efficiency of melt removal from the cut kerf. The striations observed on the stainless steel cut edges during fiber laser cutting with an inert assist gas are associated with the melt flow mechanisms. Therefore, the cutting process parameters that affect the power intensity at the cutting front and the gas dynamics in the narrow thick-section cut kerf have a great bearing on boundary layer separation, dross adherence, and the resultant cut edge surface roughness.

Surface roughness is the unevenness of the cut surface profile which is observed as striations and adherent dross on the cut edge caused by the dynamical behavior of the laser cutting process. The dynamics of the laser cutting process affects the shape of the cutting front and the melt flow mechanism. Inefficient melt removal and the geometrical shape of the lower edge of the melting front have a strong bearing on the occurrence of adherent dross and is closely related to the properties of the melt flow [30]. High surface tension and viscosity of the molten metals affect the melt ejection and can cause dross adherence on the lower cut edge.

The kerf size and assist gas pressure influence the melt velocity and melt film thickness. Dross adherence on the cut edge as indicated in Figure 7 is caused by the inefficient melt ejection at the lower cut edge because the molten metal is thicker at the bottom of the kerf due to the deceleration of the melt film. Dross adherence in cutting of thick-section stainless steel using fiber laser with an inert assist gas jet is prevented by use of high assist gas pressures and large kerf width shown in Figure 7. The cutting process parameters that influence the kerf size and gas flow dynamics in the cut kerf – such as cutting speed, focal point position, and assist gas pressure – need to be optimized for improved melt removal. A large kerf size, high assist gas pressure, and large nozzle diameter enhance gas flow rates in the thick-section cut kerfs.

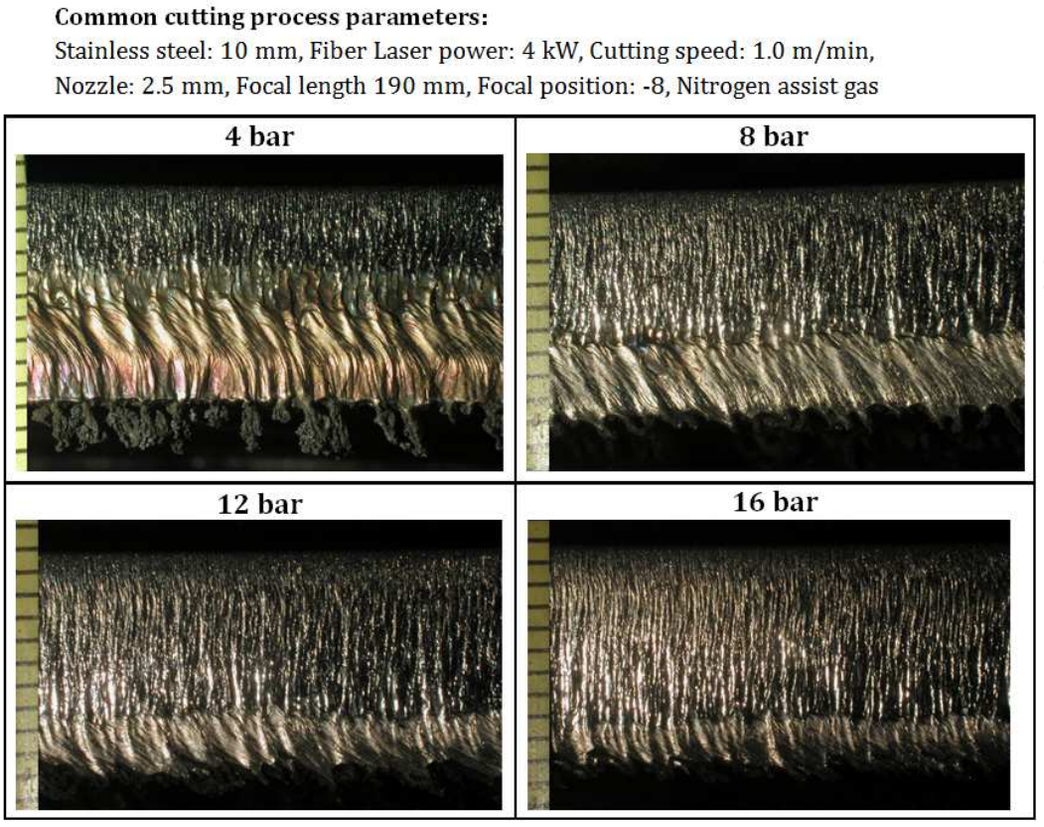

Figure 7. Effect of assist gas pressure on the location of the boundary layer separation point and dross attachment on cut edges in inert gas-assisted laser cutting

4.2.2. Categorization of the fiber laser cut edges

Wandera et al. [31] presented the different categories of the fiber laser cut edges in thick-section steel and medium-section aluminum for different cutting speeds at different power levels. There was existence of adherent dross on cut edges obtained at the slow cutting speeds and at the cutting speeds close to the maximum achievable cutting speed for a given laser power level. Wandera and Kujanpää [35] established the cutting process parameter combinations for optimization of the cut edge quality in 10-mm stainless steel workpiece. The poor cut edge quality – dross attachment and boundary layer separation – observed in thick-section stainless steel cut edges obtained using the high brightness fiber laser and an inert assist gas jet is caused by the difficulty in melt ejection through the narrow thick-section cut kerfs [32, 36]. Therefore, the rate of melt removal from the narrow thick-section cut kerf may be a potential factor limiting the maximum workpiece thickness that can be cut using the high brightness fiber laser rather than the required laser power.

4.3. Effects of laser cutting process parameters

Cutting process parameters that can be altered for the improvement of the cutting process and the resulting cut edge quality include: used laser power, cutting speed, type and pressure of

assist gas, nozzle diameter and nozzle stand-off distance, focal point position relative to the workpiece, and focal length of focusing optics. Maximum cutting speed at a given laser power level and efficient melt removal for prevention of the undesired dross adherence on the cut edge can be achieved through optimization of the cutting process parameters. Sparkes et al. [32] experimentally investigated the effects of different cutting process parameters in the cutting of 6–10 mm 304 stainless steel using a high brightness ytterbium fiber laser. Wandera et al. [23, 31] and Wandera and Kujanpää [29], also experimentally investigated the effects of process parameters in the cutting of 10-mm stainless steel, 15-mm mild steel, and 4-mm aluminum using the high brightness fiber laser. They observed that the cut edge quality in 6–10-mm stainless steel improved with increase in cutting speeds, higher nitrogen assist gas pressures, and wider cut kerfs. The cut kerf width depends on the focused spot size, laser power absorbed, and the applied cutting speed.

4.3.1. Effect of laser power and cutting speed

The maximum achievable cutting speeds increase with increase in the incident laser power used for cutting. Wandera et al. [23, 31] and Sparkes et al. [32] reported that for the cut edge quality in 6–10- mm stainless steel, the location of the boundary layer separation point moves closer to the bottom cut edge with increase in cutting speed. A lower dross attachment is experienced with high cutting speeds than when slow cutting speeds are used. The higher energy density loss from the cutting front when cutting at low cutting process increases the tendency of dross adherence on the cut edge. The cut edge quality improved with increase in cutting speeds.

There is a tendency of dross adherence on the cut edge when cutting at the maximum cutting speeds using the high brightness ytterbium fiber laser; therefore, there is need to define the acceptable cut edge quality. Typically, the cutting speed giving the best cut edge quality is lower than the maximum achievable speed for cutting through a given material at the given laser power level. Therefore, the cutting speed giving the best cut quality is the optimum cutting speed, especially for applications where cut edge quality is of paramount importance [35]. Application of cutting speeds that are beyond or below the optimum cutting speed results in dross adherence on the lower cut edge. To improve the cut quality in metal cutting using the high brightness and short wavelength lasers, Olsen et al. [37] developed a multi-beam approach to control the melt flow out of the cut kerf. Their approach involves splitting up the beams from two single mode fiber lasers and positioning the beams in a pattern in the cut kerf in such a way that there is a melt beam that performs melting and the melt ejection beam.

In reactive fusion cutting using an active assist gas jet, there is a significant variation in kerf width with cutting speed because the exothermic reaction is very erratic at slow cutting speeds, resulting in increased sideways burning and widening of the kerf width (see Figure 8). There is a reduction in the occurrence of the irregular deep grooves on the cut edge with a reduction of assist gas pressure and increase in cutting speed to optimum levels. Increased cutting speeds also result in poor melt ejection at the bottom of the cut kerf, causing dross attachment and in worst cases the eventual resealing of the lower cut edge by the resolidified melt.

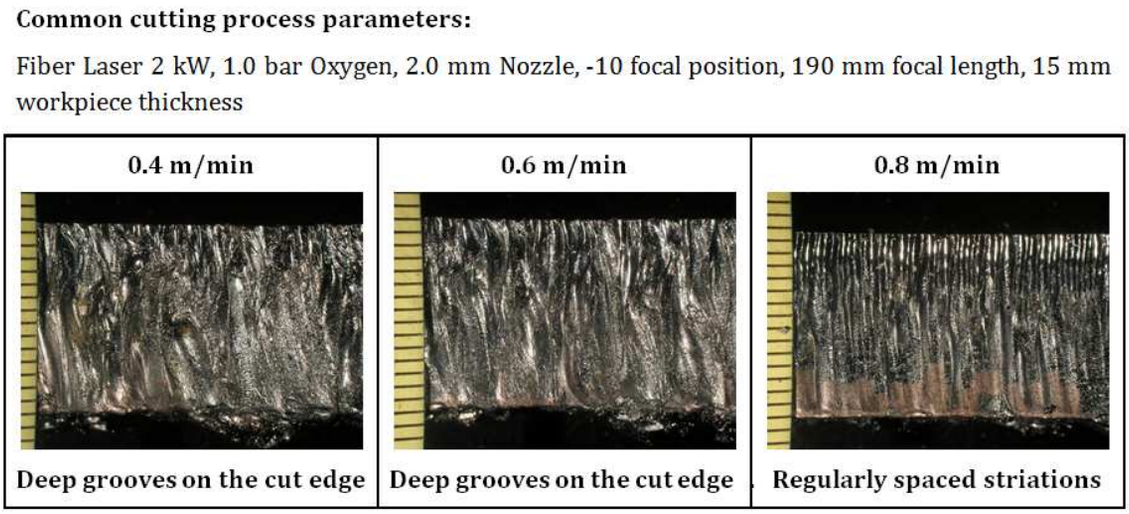

Figure 8. Effect of cutting speed on striation pattern in 15- mm mild steel

4.3.2. Effect of type and pressure of assist gas

Wandera et al. [29] showed that there was a good correlation between the calculated melt flow velocity and melt film thickness with the location of the boundary layer separation point on the 10-mm stainless steel cut edges made using a high-power fiber laser with an inert assist gas jet. The melt flow velocity increases with increasing assist gas pressure so that the melt film thickness decreases and the boundary layer separation point moves closer to the kerf bottom with increase in assist gas pressure. Consequently, in the cutting of the 10-mm stainless steel plate using the high brightness fiber laser, the cut edge quality was optimized with increase in assist gas pressure to over 16 bars so as to eliminate the boundary layer separation on the cut edge (see Figure 9). The dross attachment on the cut edge and surface roughness is also reduced with increase in assist gas pressure as shown in Figure 10. It is shown in Figure 9 that the assist gas pressure does not have an effect on the kerf width in inert gas-assisted laser cutting.

The dynamic nature of the exothermic oxidation reaction that occurs during reactive fusion laser cutting of mild steel is favored by high oxygen gas pressure resulting in wider non-uniform cut kerfs as shown in Figure 11. The nature of the erratic exothermic oxidation reaction at high oxygen pressure produces irregular deep striations on the cut edge. The ridges observed on the cut edge in laser oxygen-assisted cutting of 15-mm mild steel using the fiber laser is typical of the mechanism of the sideways burning, as originally explained by Arata et al. and Miyamoto and Maruo [38, 39].

4.3.3. Effect of focal point position

The focal point position is the location of the minimum focused spot size relative to the workpiece top surface. The focal point position which affects the laser power intensity on the workpiece influences the cut kerf size and affects the melt removal process, thus affecting the

http://dx.doi.org/10.5772/62014

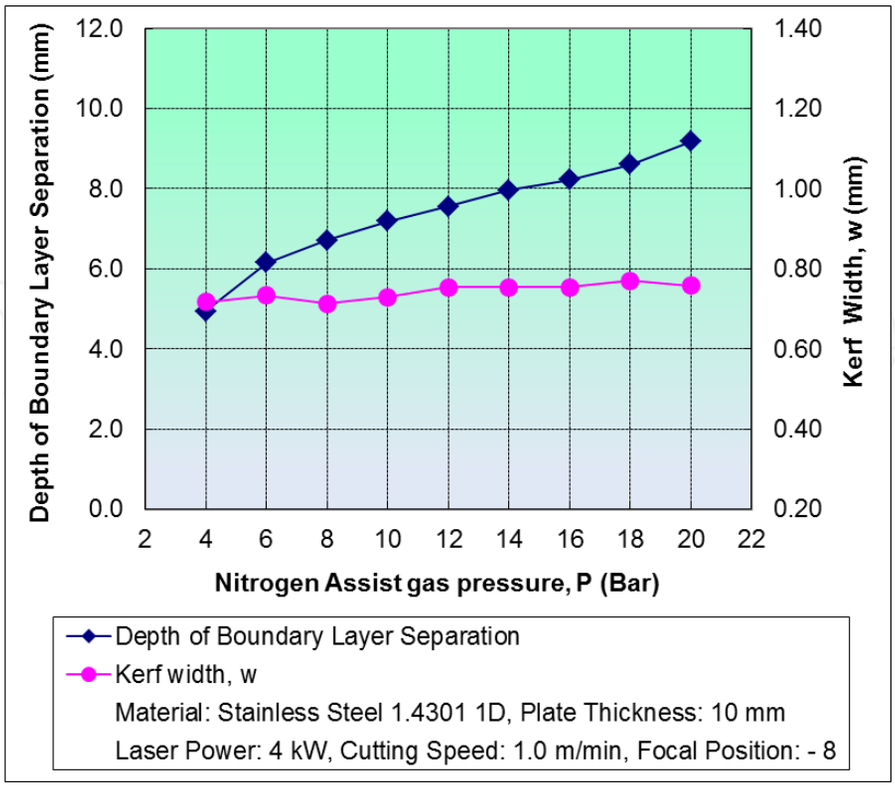

Figure 9. Effect of assist gas pressure on the location of boundary layer separation point and kerf width in inert gas-assisted laser cutting

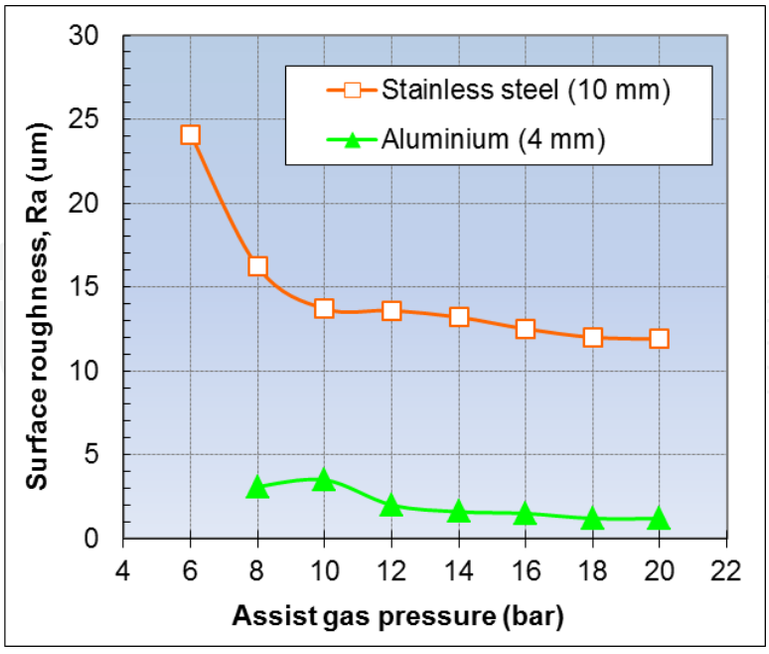

Figure 10. Variation of surface roughness with assist gas pressure for the fiber laser cut edges in 10-mm stainless steel and 4-mm aluminum

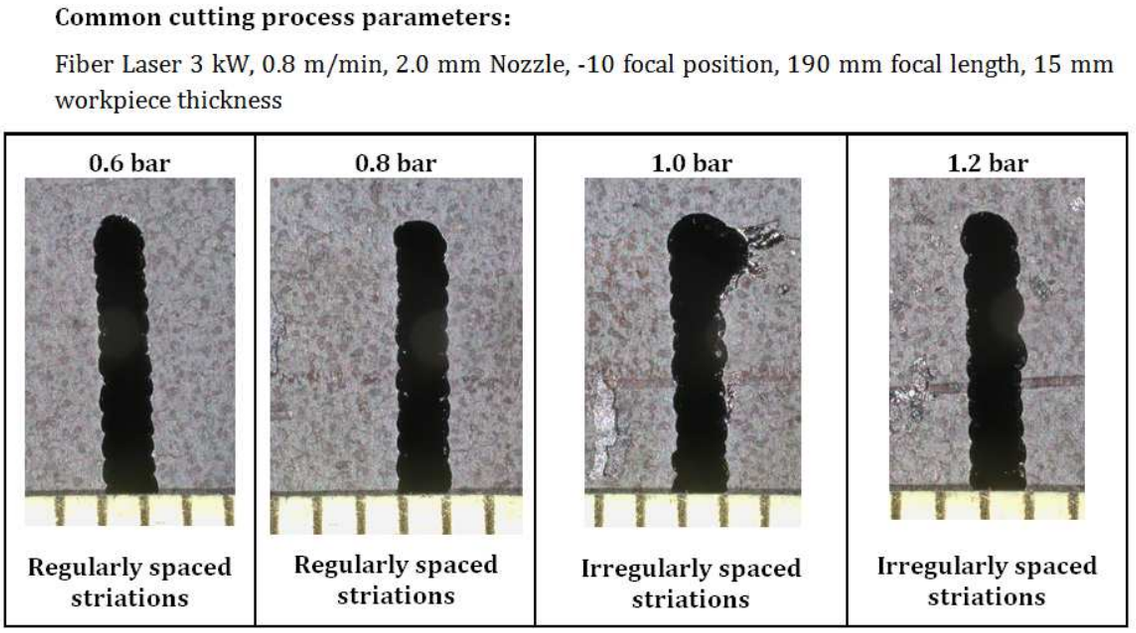

Figure 11. Effect of oxygen assist gas pressure on the kerf width and striations

cut edge quality. The highest incident power intensity necessary for penetration of a thick-section metal workpiece at the highest cutting speed is achieved when the focal position is at the workpiece top surface. However, for fiber laser cutting, the focal position at the workpiece top surface results in narrow cut kerfs and the poor melt removal mechanism in the narrow thick-section laser cut kerfs causes dross attachment on the lower cut edge. Usually, the lower section of the cut edge has a higher surface roughness than the upper section due to the melt build-up at the lower cut section, resulting in inefficient melt removal.

Efficient melt removal is obtained when wider cut kerfs are created with the focal position located below the workpiece top surface. For improved cut edge quality, the focal positions below the workpiece top surface are essential in thick-section metal cutting using the fiber laser so as to obtain wider cut kerfs for efficient melt removal as long as the power intensity at the workpiece top surface is sufficient to obtain complete penetration of the workpiece. When cutting thick-section stainless steel using the fiber laser, optimum cut edge quality is obtained when the focal position is located on the lower surface of the workpiece as long as the power intensity is sufficient to penetrate the workpiece at the applied cutting speed; in this case, the applied cutting speed should be lower than the maximum achievable speed for the applied laser power. Complete penetration of the thick-section stainless steel workpiece cannot be achieved at the maximum cutting speed for a given power level when the focal point position is far into the lower half section of the workpiece thickness because of the reduced power intensity on the workpiece surface. On the cutting of a 10-mm stainless steel workpiece using the fiber laser, the tendency for dross attachment on the lower cut edge is more significant with focal point positions located on the upper half section of the workpiece thickness (see Figure 12). Focal positions close to the workpiece bottom surface produce clean dross-free cuts because of the wider cut kerfs formed with these focal positions.

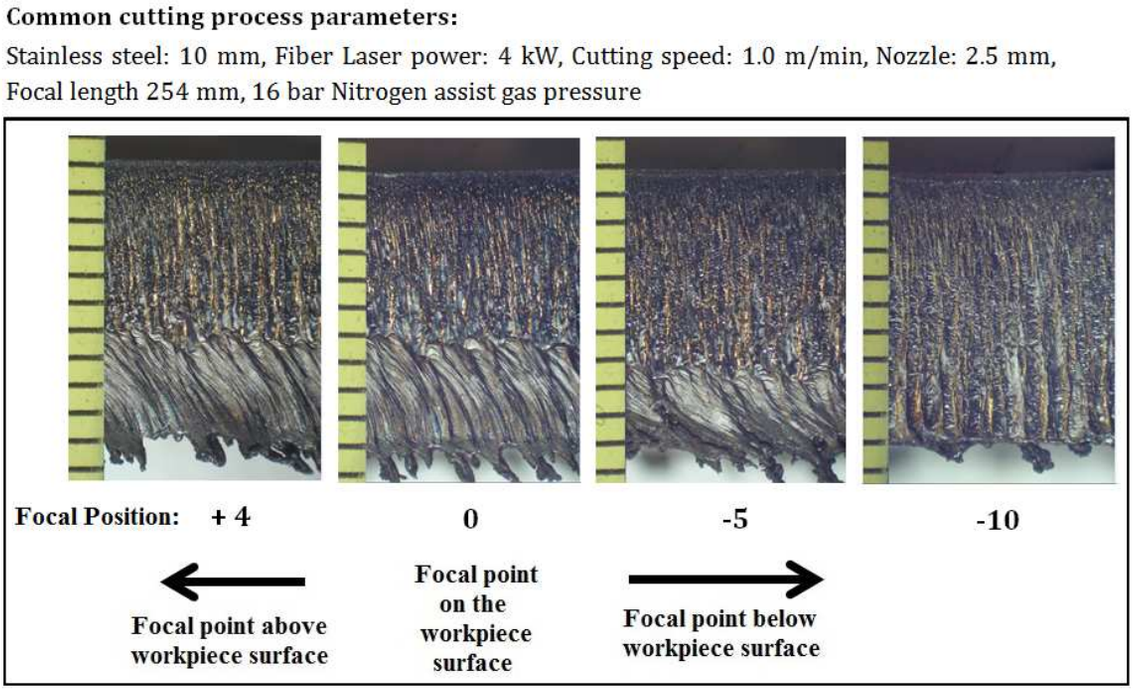

Figure 12. Effect of focal point position on the dross adherence on 10-mm stainless steel

4.3.4. Effect of nozzle diameter and stand-off distance

The efficiency of melt ejection is influenced by the nozzle diameter which determines the amount of the cutting gas jet available at the cutting front. In the case of thick-section metal cutting with an inert assist gas jet, the nozzle diameter significantly affects the location of the boundary layer separation point on the cut edge. The location of the boundary layer separation point moves toward the bottom cut edge with increase in the nozzle diameter because of the enhanced melt removal process facilitated by the increased amount of assist gas provided by the large-size nozzle. There is no boundary layer separation on the cut edge with the 2.5-mm nozzle diameter [29].

In the oxygen-assisted laser cutting, a smaller nozzle size enhances achievement of a good cut quality with a finer uniform striation pattern on the cut edge by limiting the extent of the sideways burning oxidation reaction. In fiber laser cutting of 15-mm mild steel using oxygen assist gas, the best cut quality was obtained with a 1.5-mm nozzle diameter and the 2.5-mm nozzle diameter produced the worst cut edge quality [23].

The nozzle stand-off distance – distance between the nozzle and the workpiece top surface – influences the gas flow dynamics at the entrance of the cut kerf and consequently affects the gas flow patterns at the cutting front. The gas flow patterns at the cutting front have a strong effect on the resulting cut edge quality especially during high pressure inert gas-assisted laser cutting [40, 41, 42]. The nozzle stand-off distances (0.5–1.2 mm) tested by Wandera and Kujanpää [29] in the cutting of 10-mm stainless steel workpiece showed that the nozzle stand-off distance did not have an effect on the location of boundary layer separation [29].

4.3.5. Effect of focal length of focusing optics

The effects of cutting speed and focal point position on the surface roughness of the fiber laser cut edges are more significant when a short focal length of the focusing optics is used than when longer focal length optics is used. In cutting of 10-mm stainless steel using the 4 kW fiber laser power at cutting speed of 1.0 m/min and focal position located on the bottom workpiece surface, dross-free cut edges with lower surface roughness were obtained with the 254-mm focal length optics than when the 190.5-mm focal length optics was used. This is because wider cut kerfs were obtained with the 254-mm focal length optics compared to the 190.5-mm focal length optics [35].

5. Conclusion

Performance of the high brightness ytterbium fiber laser system in metal cutting has been extensively evaluated in stainless steel, mild steel and aluminium cutting. The maximum cutting speeds and maximum workpiece thickness that can be cut using the ytterbium fiber laser have been shown to be largely governed by a number of cutting process parameters that affect the melt removal process and influence the resultant cut edge quality. Exceedingly higher cutting speeds in thin-section to medium-section (less than 6 mm sheet thickness) metal cutting have been realized with the ytterbium fiber laser compared to the CO_2 laser. However, a drastic reduction in maximum cutting speed has been reported in thick-section (above 6 mm sheet thickness) metal cutting using the ytterbium fiber laser due to deterioration in cut edge quality at the maximum cutting speed. Optimization of the cutting process parameters for enhancement of the cut edge quality in thick-section metal cutting at high cutting speeds using the ytterbium fiber laser has shown that the maximum applicable cutting speed is influenced by the melt removal process.

Acknowledgements

The company HT Laser Oy is acknowledged for funding the fiber laser experimental work which formed a basis for analysis of the performance of the high brightness ytterbium fiber laser in metal cutting that is presented in the Chapter on Fiber Lasers in Materials Processing. Lappeenranta Laser Processing Center at Lappeenranta University of Technology in Finland is acknowledged for facilitation of the fiber laser experimentation. Professor Veli Kujanpää of VTT Technical Research Centre of Finland and Professor Antti Salminen of Lappeenranta University of Technology are acknowledged for the invaluable discussions that inspired the formulation of the ideas presented in this chapter. I also acknowledge Busitema University, Faculty of Engineering, for providing a conducive environment during the preparation of this book chapter.

Author details

Catherine Wandera*

Address all correspondence to: cathywandera@yahoo.com

Busitema University, Tororo, Uganda

References

[1] Petring D, Schneider F, Wolf N, Nazery V. The relevance of brightness for high power laser cutting and welding. Proc. 27th Int. Congr Applic Lasers Electro Optics, ICALEO 2008 (October 20-23), Temecula, California, USA, paper 206, 2008;95–103.

[2] Müller H-R, Kirchhof J, Reichel V, Unger S. Fibers for high-power lasers and amplifiers. Comptes Rendus Physique 2006;7(2):154 –62.

[3] Hügel H. New solid-state lasers and their application Potentials. Optics Lasers Eng 2006;34(4–6):213 –29.

[4] Canning J. Fiber lasers and related technologies. Optics Lasers Eng 2006;44(7):647 –76.

[5] Nilsson J, Clarkson WA, Selvas R, Sahu JK, Turner PW, Alam S-U, Grudinin AB. High-power wavelength-tunable cladding-pumped rare-earth-doped silica fiber lasers. Optical Fiber Technol 2004;10(1):5 –30.

[6] Jarman RH. Novel optical fiber lasers. Curr Opin Solid State Mater Sci 1996;1(2):199 –203.

[7] Limpert J, Schreiber T, Liem A, Nolte S, Zellmer H, Peschel T, Guyenot V., Tünnermann A. Thermo-optical properties of air-clad photonic crystal fiber lasers in high power operation. Optics Express 2003;11(22):2982 –90.

[8] Hecht J. Photonic Frontiers: Fiber Lasers: Fiber lasers ramp up the power. [In OptoIQ www-pages], [retrieved May 5, 2009]. From: http://www.optoiq.com/index/photonics-technologies-applications/lfw-display/lfw-article-display/371319/articles/laser-focus-world/volume-45/issue-12/features/photonic-frontiers-fiber-lasers-fiber-lasers-ramp-up-the-power.html).

[9] O'Neill W, Sparkes M, Varnham M, Horley R, Birch M, Woods S, Harker A. High power high brightness industrial fiber laser technology. Proc 23rd Int Congr Applic Lasers Electro Optics, ICALEO 2004 (October 4–7), San Francisco, California, USA, paper 301, 2004;1–7.

[10] Thomy C, Seefeld T, Vollertsen F. High-power fiber lasers – application potentials for welding of steel and aluminium sheet material. Adv Mater Res 2005;6–8:171–8, available online at http://www.scientific.net/

[11] Kancharla V. Applications review: materials processing with fiber lasers under 1kW. Proc 25th Int Congr Applic Lasers and Electro Optics, ICALEO 2006 (October 30–November 2), Scottsdale, Arizona, USA, Paper 1301, 2006;579–85.

[12] Quintino L, Costa A, Miranda R, Yapp D, Kumar V, Kong CJ. Welding with high power fiber lasers – a preliminary study. Mater Design 2007;28(4):1231 –7.

[13] Jeong Y, Sahu JK, Payne DN, Nilsson J. Ytterbium-doped large-core fiber laser with 1.36 kW continuous-wave output power. Optics Express 2004;12(25):6088 –92.

[14] IPG Photonics. Materials Processing: Single mode fiber lasers, Multi mode fiber lasers. [In IPG Photonics www-pages], [retrieved May 10, 2010]. From http://www.ipgphotonics.com/apps_materials.htm

[15] Steen WM. Laser Material Processing, 3rd edn. Springer-Verlag, London, 2003, pp. 83–90, 111–122, 126, 163–165.

[16] Powell J. CO_2 Laser Cutting, 2nd edn, Chapter 1: Section 1.2. Springer, London Ltd, 1998.

[17] Rémy F, Sonia S, Frédéric C, Francis B, Bruno D, Guillaume L. Analysis of basic processes inside the keyhole during deep penetration Nd-Yag Cw laser welding. Proc 25th Int Congr Applic Lasers Electro-Optics ICALEO 2006, 30th October –2nd November 2006, Scottsdale, Arizona, USA.

[18] Salminen A, Fellman A. The effect of laser and welding parameters on keyhole and melt pool behavior during fiber laser welding. Proc 26th Int Conf Lasers Electro Optics ICALEO2007, Orlando, FL, USA, October 29–November 1, 2007.

[19] Olsen FO. Fundamental mechanisms of cutting front formation in laser cutting. Proc SPIE, 2207, 1994;235–47.

[20] Olsen FO. Cutting front formation in laser cutting. Annal CIRP 1989;38(1):215–8.

[21] Yilbas BS. Laser heating process and experimental validation. Int J Heat Mass Transfer 1997;40(5):1131 –43.

[22] Duan J, Man HC, Yue TM. Modeling the laser fusion cutting process: I. Mathematical modelling of the cut kerf geometry for laser fusion cutting of thick metal. J Physics D Appl Phys 2001;34(14):2127 –34.

[23] Wandera C, Kujanpää V, Salminen A. Laser power requirement for cutting of thick-section steel and effects of processing parameters on mild steel cut quality. Proc IMechE B, J Eng Manufacture 2011;225:651–61.

[24] Schulz W, Becker D, Franke J, Kemmerling R, Herziger G. Heat conduction losses in laser cutting of metals. J Phys D Appl Phys 1993;26(9):1357 –63.

[25] Ion JC. Laser Processing of Engineering Materials: Principles, Procedure and Industrial Application. Elsevier Butterwort-Heinemann, 2005.

[26] Powell J, Petring D, Kumar RV, Al-Mashikhi SO, Kaplan AFH, Voisey KT. Laser-oxygen cutting of mild steel: the thermodynamics of the oxidation reaction. J Phys D Appl Phys 2009;42(1):1 –11.

[27] Ready JF, Farson DF. (Eds). LIA Handbook of Laser Materials Processing. Laser Institute of America, 2001.

[28] Xie J, Kar A, Rothenflue JA, Latham WP. Temperature-dependent absorptivity and cutting capability of CO_2, Nd: YAG and chemical oxygen-iodine lasers. J Laser Applic 1997;9(2):77–85.

[29] Wandera C, Kujanpää V. Characterization of the melt removal rate in laser cutting of thick-section stainless steel. J Laser Applic 2010;22(2):62–70.

[30] Schulz W, Kostrykin V, Nießen M, Michel J, Petring D, Kreutz EW, Poprawe R. Dynamics of ripple formation and melt flow in laser beam cutting. J Phys D Appl Phys 1999;32(11):1219 –28.

[31] Wandera C, Salminen A, Kujanpää V. Inert gas cutting of thick-section stainless steel and medium-section aluminium using a high power fiber laser. J Laser Applic 2009;21(3):154–61.

[32] Sparkes M, Gross M, Celotto S, Zhang T, O'Neill W. Practical and theoretical investigations into inert gas cutting of 304 stainless steel using a high brightness fiber laser. J Laser Applic 2008;20(1):59 –67.

[33] Wandera C, Salminen A, Kujanpää V, Olsen F. Cutting of stainless steel with fiber and disk laser, 2006, 10 pages, Proc 25th Int Congr Applic Lasers Electro-Optics ICALEO 2006, 30th October – 2nd November 2006, Scottsdale, Arizona, USA.

[34] European Committee for Standardization. Thermal cutting – Classification of thermal cuts, Geometrical product specification and quality tolerances. EN ISO 9013: 2002 (SFS-ISO EN 9013:2002.

[35] Wandera C, Kujanpää V. Optimization of parameters for fiber laser cutting of a 10 mm stainless steel plate, Proc IMechE Part B, J Eng Manufacture 2011;225:641–9.

[36] Sparkes M, Gross M, Celotto S, Zhang T, O'Neill W. Inert cutting of medium section stainless steel using a 2.2 KW high brightness fiber laser. Proc 25th Int Congr Applic Lasers Electro Optics, ICALEO 2006 (October 30 – November 2), Scottsdale, Arizona, USA, paper 402, 2006;197–205.

[37] Olsen FO, Hansen KS, Nielsen JS. Multibeam fiber laser cutting. J Laser Applic 2009;21(3):133 –8.

[38] Arata Y, Maruo H, Miyamoto I, Takeuchi S. Dynamic behavior in laser gas cutting of mild steel. Transac JWRI 1979;8:15–26.

[39] Miyamoto I, Maruo, H. The mechanism of laser cutting. Weld World (UK) 1991;29:283–94.

[40] Fieret J, Terry MJ, Ward BA. Overview of flow dynamics in gas-assisted laser cutting. Paper presented to the Fourth International Symposium on Optical and Optoelectronic Applied Science and Engineering, Topical Meeting on High Power Lasers: Sources, Laser-Material Interactions, High Excitations, and Fast Dynamics in Laser Processing and Industrial Applications, 1987 (March 30 – April 3), The Hague, The Netherlands.

[41] Zefferer H, Petring D, Beyer E. Investigation of the gas flow in laser beam cutting. Lectures and Posters of the 3rd International Beam Technology Conference, Karlsruhe, 1991 (March 13–14).

[42] Man HC, Duan J, Yue TM. Behaviour of supersonic and subsonic gas jets inside laser cut kerfs. Proc of ICALEO 1997, San Diego, USA, B27-36.